RESEARCH ARTICLE

PLANETARY GEOLOGY

Cassini finds molecular hydrogen in the Enceladus plume: Evidence for hydrothermal processes

J. Hunter Waite,[1*] Christopher R. Glein,[1*] Rebecca S. Perryman,[1] Ben D. Teolis,[1] Brian A. Magee,[1] Greg Miller,[1] Jacob Grimes,[1] Mark E. Perry,[2] Kelly E. Miller,[1] Alexis Bouquet,[1] Jonathan I. Lunine,[3] Tim Brockwell,[1] Scott J. Bolton[1]

Saturn's moon Enceladus has an ice-covered ocean; a plume of material erupts from cracks in the ice. The plume contains chemical signatures of water-rock interaction between the ocean and a rocky core. We used the Ion Neutral Mass Spectrometer onboard the Cassini spacecraft to detect molecular hydrogen in the plume. By using the instrument's open-source mode, background processes of hydrogen production in the instrument were minimized and quantified, enabling the identification of a statistically significant signal of hydrogen native to Enceladus. We find that the most plausible source of this hydrogen is ongoing hydrothermal reactions of rock containing reduced minerals and organic materials. The relatively high hydrogen abundance in the plume signals thermodynamic disequilibrium that favors the formation of methane from CO_2 in Enceladus' ocean.

In hydrothermal systems on Earth, water reacts with rocks containing reduced iron-bearing minerals to produce molecular hydrogen (*1*, *2*). Reduced iron acts as an oxygen sink, providing sufficient reduction potential to drive the conversion of some H_2O to H_2. Because of rapid convective transport of fluids in these dynamic systems, hydrothermally derived H_2 is far from chemical equilibrium when it mixes with oxidants in the cooler surrounding environment [e.g., seawater (*3*, *4*)]. This state of disequilibrium is exploited by some forms of life (chemolithotrophs) as a source of chemical energy. One example is microorganisms that obtain energy by using H_2 to produce CH_4 from CO_2 in a process called methanogenesis. Such H_2-based metabolisms are used by some of the most phylogenetically ancient forms of life on Earth (*5*). On the modern Earth, geochemically derived fuels such as H_2 support thriving ecosystems (*6*–*8*) even in the absence of sunlight.

Previous flybys of the saturnian satellite Enceladus by the Cassini spacecraft provided evidence for a global subsurface ocean residing above a core of rocky material (*9*–*12*). The inference of warm water cycling through silicates at the base of this ocean (*13*) raises the issue of whether this geologically active moon of Saturn—which ejects gases and ice grains through a system of fractures to form a plume (*14*)—might have active hydrothermal systems. Molecular hydrogen would be produced during hydrothermal alteration of reduced chondritic rock and could be observable in the plume gas (*15*, *16*). Hence, H_2 may serve as a marker of hydrothermal processes, although other sources of H_2 (e.g., ice radiolysis) must be considered before a hydrothermal origin can be deduced. The presence of H_2 in the plume of Enceladus could therefore suggest the occurrence of temperatures and chemical energy sources necessary for habitable conditions in the moon's interior (*17*).

For the final Cassini in situ flyby of Enceladus (designated E21), the Open Source Neutral Beaming (OSNB) mode of the Ion Neutral Mass Spectrometer [INMS (*18*)] was used to search for native H_2 in the plume. The open source is a direct inlet into the mass spectrometer that minimizes gas interaction with the walls of the instrument before analysis in the quadrupole mass spectrometer. OSNB mode ameliorates the issue of hydrogen production inside the instrument from water-titanium interactions, which occurs when the alternative Closed Source Neutral (CSN) mode is used (*19*). The use of OSNB mode during E21 permits a more straightforward interpretation of the data regarding the presence of H_2 at Enceladus.

Final observations and analysis of plume gas

All close Cassini Enceladus flybys are designated according to their order of occurrence (E1, E2, etc.). INMS performed measurements of the Enceladus plume during eight flybys: the south-to-north discovery flyby E2 [year 2005–day 195 (*14*)]; the north-to-south E3 (2008-072) and E5 (2008-283) flybys (*19*), which flew close to the plume axis outbound from Enceladus; a series of low-altitude plume traversals, E7 (2009-306), E14 (2011-274), E17 (2012-087), and E18 (2012-105); and most recently E21 (2015-301), which was the deepest observation within the plume at a closest approach of 49 km from the surface.

During the E21 flyby, Cassini flew almost perpendicular to the Enceladus tiger stripes at a relative speed of 8.5 km s^{-1}. The INMS sensor alternated between two different modes of operation. CSN mode increases the total signal by collecting and thermally equilibrating ("thermalizing") gas in a titanium antechamber prior to ionization, mass selection, and detection. OSNB mode directly samples ambient gas, ionizing the neutral beam as it travels through the instrument without striking the walls. The use of OSNB mode during the INMS observations of E21 on 28 October 2015 enabled the detection and quantification of H_2 in the plume.

OSNB mode has a set of deflector elements that prevent ion entry, as well as a velocity filter that accepts incoming neutral molecules over a narrow but adjustable range of angles and energies after they are ionized in the ion source. Although it has only 0.25% of the sensitivity of CSN mode, OSNB mode minimizes the measurement of molecules that are generated by surface interactions on the walls of the CSN antechamber. In OSNB mode, neutral molecules are ionized and analyzed without contacting instrumental surfaces (*18*).

The velocity vector of the molecules on arrival at the OSNB aperture determines their apparent energy in relation to the spacecraft. During E21, the electrostatic velocity filter was continuously adjusted via sawtooth scans of ±2 km s^{-1} in amplitude to characterize the velocity distribution of the plume gas and consequently to accept molecules arriving from the direction of Enceladus' surface (fig. S9). In addition to OSNB measurements, CSN data were acquired to determine whether there were any major changes in plume composition relative to the earlier E14, E17, and E18 flybys.

The E21 INMS data are shown in Fig. 1. A large number of mass 2 counts were detected in OSNB mode, potentially indicating the presence of H_2 in the plume. However, background (instrumental) sources of mass 2 counts must be considered to determine whether native H_2 is present.

We investigated sources of background [(*20*), section 1] and found that the main source of background is leakage of thermalized background H_2O gas from the rest of the instrument into the open source [fig. S4; see also (*21*)]. Other background sources include thermal leakage of H_2 from the rest of the instrument into the open source, dissociative ionization of the incoming H_2O molecular beam in the open source, radiation noise in the detector, and leakage of ions from the closed source through the quadrupole switching lens. We quantified the background sources by applying calibration data from literature and laboratory experiments with the INMS engineering model to the observed mass 18 OSNB counts and to the mass 2 and mass 18 CSN counts [(*20*), section 1].

The estimated background is plotted with the raw mass 2 data in Fig. 2. The >1σ difference between the observed counts and the total background

[1]Space Science and Engineering Division, Southwest Research Institute, 6220 Culebra Road, San Antonio, TX 78238, USA. [2]Applied Physics Laboratory, Johns Hopkins University, Laurel, MD 20723, USA. [3]Department of Astronomy and Carl Sagan Institute, Cornell University, Ithaca, NY 14853, USA.
*Corresponding author. Email: hwaite@swri.edu (J.H.W.); cglein@swri.edu (C.R.G.)

Downloaded from http://science.sciencemag.org/ on April 13, 2017

over multiple measurements suggests a contribution of native H_2 in the Enceladus plume to the signal.

The data show a low-level H_2 population together with several extreme H_2 signal spikes reaching intensities of tens to hundreds of counts (Fig. 2). The empirical distribution of the background-subtracted mass 2 counts at or below 10 counts is closely approximated by a normal distribution (Fig. 3; Shapiro-Wilk normality test statistic of W = 0.97 yields a *P* value of 0.20). The generalized extreme Studentized deviate (ESD) test for outliers was performed (α = 5% level; upper bound of 10 outliers considered) on the complete set of background-subtracted data from −1 s to +4 s from closest approach. The test revealed eight outliers in the data set (determined by finding the largest number of outliers in which the corresponding test statistic, 3.4, is greater than the associated critical value for α = 5%, 3.2). The statistical outliers correspond to the points (spikes) above 10 counts.

These spikes are difficult to attribute to plume spatial structure, which would require changes in H_2 density of one to two orders of magnitude within a 1-km spatial extent (or 0.1 s in duration) parallel to the spacecraft trajectory. Possible explanations for the mass 2 spikes include intermolecular collisions and scattering of ambient H_2 off of H_2O gas/grain jets, or H_2 scattering from stream-stream ineractions between multiple gas jets. Because the spikes are outliers and it is currently unclear how their production should be modeled, they are not included in our determination of the plume's H_2/H_2O ratio. Nonetheless, they constitute approximately half of the observed mass 2 counts.

The background-subtracted H_2 signal below 10 counts can be used to estimate the mixing ratio of H_2 in the ejected plume vapor. This modeling convolves the OSNB velocity and angular response determined from ray tracing [(*20*), section 2.2] with the spatial and velocity distribution of H_2 ejected from gas sources along the tiger stripes corrected for spacecraft altitude [(*20*), section 2.3]. We considered two general models of plume outflow. In the isotropic model, the H_2 velocity distribution is homogenized by intermolecular collisions and scattering from the heavier and more abundant H_2O. In the collisionless model, H_2 arrives at the spacecraft along ballistic trajectories from the tiger stripes. The data do not indicate a clear preference between these models (fig. S12), but because the molecular mean free path (~10 km at the measured plume densities) is of smaller dimension than the spacecraft altitude (Fig. 1), collisions are expected and the isotropic model is more theoretically consistent. Therefore, we used the isotropic model to estimate the number ratio of H_2/H_2O plume vapor source rates from OSNB data acquired from −1 s to +4 s from closest approach [(*20*), section 2.3]. In addition to the mixing ratio of H_2, Table 1 provides corresponding values for CO_2, CH_4, and NH_3 derived from the average of the E14, E17, and E18 encounters, which were found to be consistent with the CSN measurements from E21 (table S2). This consistency allows us to establish a reproducible volatile content of the plume [compare with (*14*, *19*)].

The origin of H_2

We consider the plausibility of a preexisting reservoir in the ice shell or global ocean of Enceladus supplying H_2 to the plume. Molecular hydrogen is too volatile to be stored in an active ice shell, as pressures there [tens of bars (*11*)] are not high enough to form clathrate hydrates of H_2 [>1000 bar (*22*, *23*)]. Possible mixed clathrates could not provide a measurable contribution of H_2, because they would be too H_2-poor [$H_2/(CH_4 + CO_2) \approx 0.001$ to 0.05] to account for the relatively high ratio of $H_2/(CH_4 + CO_2) \approx 0.4$ to 3.5 observed in the plume [(*20*), section 4.1.2]. The derived H_2/H_2O ratio in the plume gas (Table 1) corresponds to a release rate of 1×10^9 to 5×10^9 mol H_2 year^{-1} for a water vapor emission rate of ~200 kg s^{-1} in the plume (*24*). Enceladus' ocean does not appear to contain sufficient H_2 to sustain this rate. From geochemical modeling, the ocean source of the plume (*25*, *26*) is estimated to have an H_2 concentration of ~10^{-7} to 10^{-4} mol (kg H_2O)$^{-1}$ (table S11). For an ocean mass of ~10^{19} kg (*27*), the residence time of H_2 is <1 million years. Hence, the ocean is not a robust long-term reservoir of H_2.

The observed H_2 is unlikely to have been acquired in its present chemical form from the formation environment of Enceladus. Gravitational capture of nebular gas can be ruled out because of the low gravity of Enceladus and the subsolar $^4He/H_2$ ratio in the plume [protosolar ≈ 0.2, plume < 0.015; (*20*), section 4.1.1]. The nondetection of ^{36}Ar, CO, and N_2 (table S4) implies that plausible icy building blocks of Enceladus [similar to known comets (*28*)] did not form at low enough temperatures to trap sufficient amounts of primordial H_2 (*29*), ruling out accreted cold amorphous ices as a source of plume H_2 [(*20*), section 4.1.2]. Indeed, the ice shell of Enceladus cannot robustly store

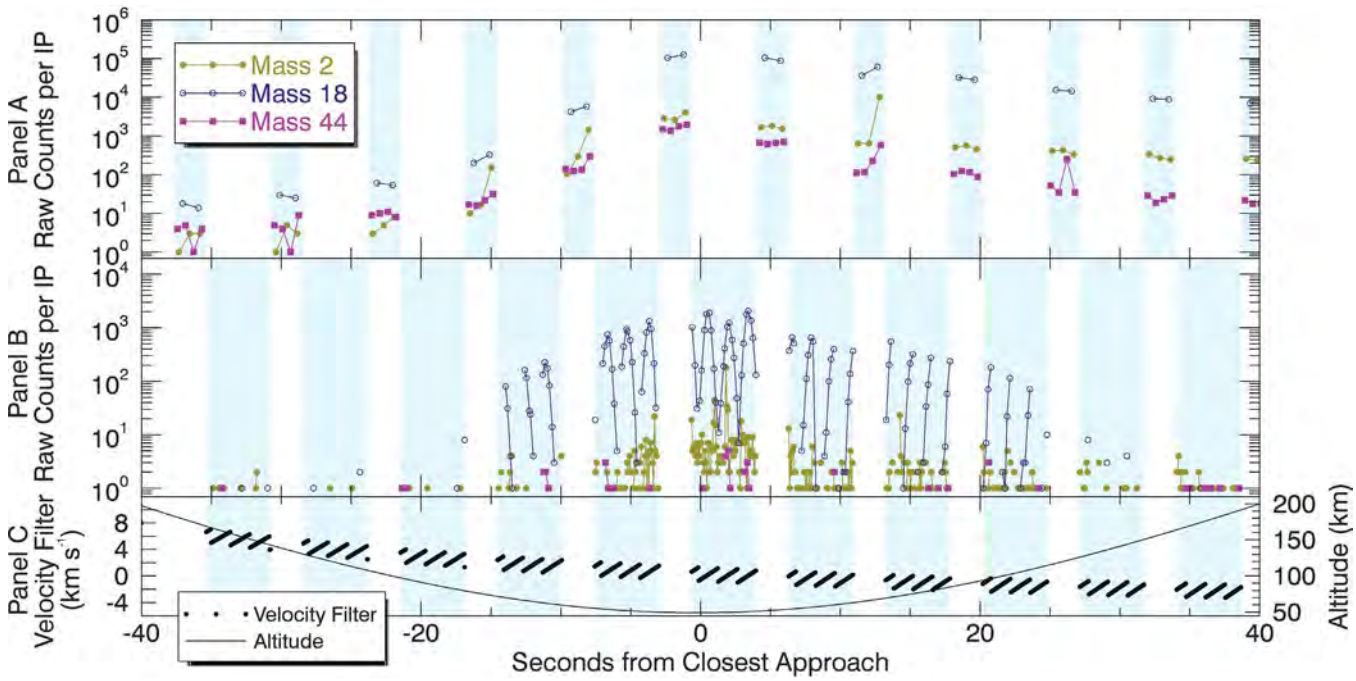

Fig. 1. Observations of H_2, H_2O, and CO_2 by INMS during the E21 flyby. (**A**) Mass 2 (H_2), mass 18 (H_2O), and mass 44 (CO_2) measurements made in CSN mode as counts per integration period (IP); INMS collects 31 ms of signal at each mass. (**B**) Interleaved OSNB measurements for the same three masses. (**C**) The velocity range sampled (black points), which corresponds to the field of view of the sampled region and affects both the speed and angle of the measured molecules. The altitude from Enceladus is also shown (black curve). The ordinate in (A) and (B) provides the number of detector ion counts in the indicated unitary mass-to-charge channel of the quadruple mass analyzer during the IP. The abscissa denotes the time of the observation relative to closest approach to Enceladus.

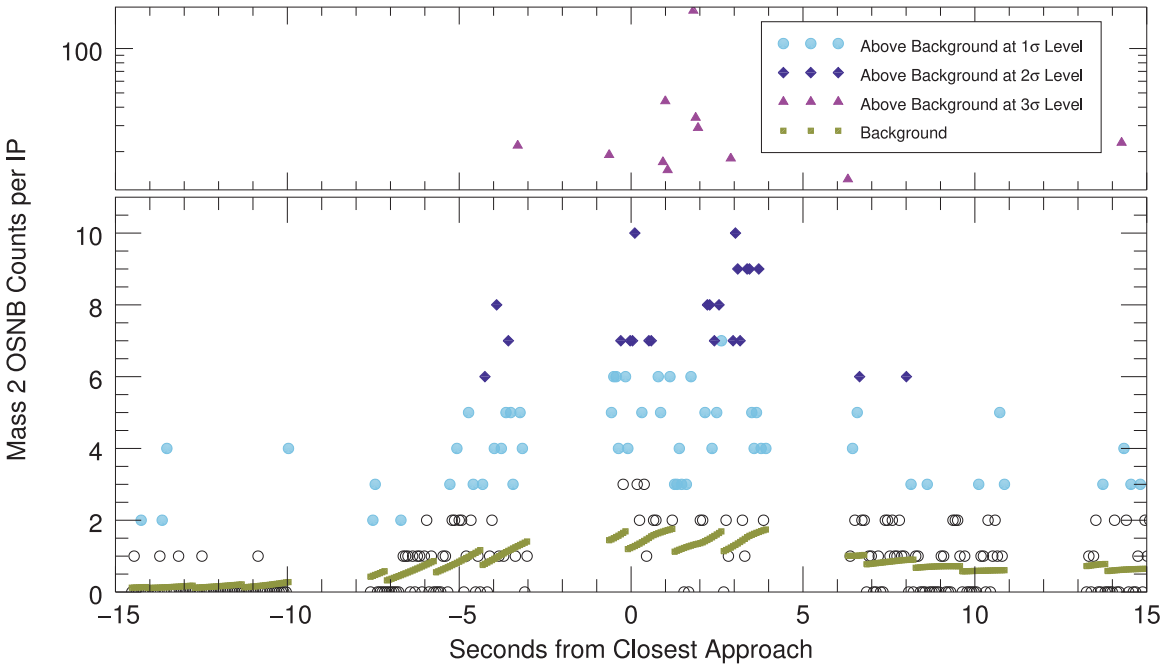

Fig. 2. Comparison of OSNB measurements of mass 2 (H_2) with the estimated total mass 2 instrumental background. The detected count rates and estimated background rates are plotted as a function of time from closest approach to Enceladus. The bottom panel of the plot is on a linear scale showing all the data points at or below 10 counts; the top panel, plotted on the common log scale, shows the remaining data points that are above 10 counts. Data points are color-coded according to the statistical uncertainties and background estimation: open black circles, no distinguishable separation from the background signal; light blue circles, at least 1σ separation; dark blue diamonds, at least 2σ separation; purple triangles, at least 3σ separation.

Table 1. The major species composition of Enceladus' plume gas. Volume mixing ratios are derived from Cassini INMS measurements [(*20*), sections 2.4 and 3.2].

Constituent	Mixing ratio (%)
H_2O	96 to 99
CO_2	0.3 to 0.8
CH_4	0.1 to 0.3
NH_3	0.4 to 1.3
H_2	0.4 to 1.4

accreted H_2 over geologic time. The observed H_2 must have been produced on Enceladus.

Chemical processes that dissociate H_2O from the ice shell appear incapable of generating sufficient H_2 to explain the observed release rate. Radiolysis of water ice at the surface of Enceladus by magnetospheric plasma is estimated to produce only ~10^7 mol H_2 year^{-1} in the south polar region [(*20*), section 4.2.3.1]. Because the radiolytic production is fairly uniformly spread geographically, this mechanism would yield a nearly global distribution of H_2. Radiolysis would also produce O_2 such that the O_2/H_2 ratio should be ~0.5. However, neither of these characteristics are observed [(*20*), section 3.3]. Shearing of water ice mixed with silica particles along the tiger stripe faults could generate H_2 according to the experiments of (*30*). However, the ice on Enceladus may be too silica-poor (*13*) to permit appreciable production of H_2. A model of this process using data from (*13*, *30*) suggests an upper limit of 4×10^4 mol year^{-1} for steady-state production of H_2 [(*20*), section 4.2.4], which is far below the release rate of H_2 in the plume (1×10^9 to 5×10^9 mol year^{-1}).

This logic implicates a source of H_2 in the rocky core of Enceladus. If the core has a low density (*9*, *10*) partly due to the presence of liquid water trapped in pore space (table S9), H_2 could be generated by radiolysis of H_2O in the core from the decay of long-lived radionuclides (*31*). However, calculations based on an adaptation of the model from (*32*) to a hydrated chondritic core inside Enceladus suggest that contemporary radiolysis could contribute ≤10^8 mol H_2 year^{-1} [(*20*), section 4.2.3.2], which would be a minor component of the observed H_2. Alternatively, a larger current contribution from subsurface radiolysis is possible if H_2 can accumulate in an impermeable core and undergo episodic release. However, storage of H_2 in the presence of potential carbon sources and metallic catalysts in the core over long periods of time may result in abiotic synthesis of CH_4 (*33*). If so, $H_2/CH_4 \approx 1$ to 14 in the plume may be too high to permit appreciable input of stored H_2 to the plume [(*20*), section 4.3].

Hydrothermal reactions between water and rock can continuously produce prodigious amounts of H_2, as observed at submarine hydrothermal systems on Earth such as Lost City (*34*). On Enceladus, hydrothermal H_2 could be produced by cracking of NH_3, by pyrolysis of accreted CHON organic materials, or by aqueous oxidation of reduced minerals [e.g., Fe^0, Fe(II)-bearing silicates]. Cracking of NH_3 would produce N_2, which is not observed in the plume; this suggests minimal input from this mechanism [(*20*), section 4.2.2]. Mass balance calculations show that the other options both have high H_2-generating potential, with theoretical yields up to ~3.5×10^{19} mol for organics and ~20×10^{19} mol for minerals in the Mg-Si-Fe-S-O-H system [(*20*), sections 4.2.1 and 4.2.5, respectively]. For context, 6×10^{18} to 2×10^{19} moles of H_2 would be required to sustain the observed rate of H_2 release throughout solar system history (4.56 billion years). These values illustrate that both processes could be important sources of H_2 because they can maintain H_2 outgassing for geologically relevant periods (e.g., hundreds of millions of years), even if the actual yields were to be substantially smaller than their maximal values [e.g., if Fe(II) is stabilized in carbonates or aluminosilicates in Enceladus' core; (*20*), section 4.2.5].

The robustness of these rocky sources of H_2, the inconsistencies of numerous alternative sources, and the earlier discovery of SiO_2 nanoparticles by the Cassini Cosmic Dust Analyzer [CDA (*13*)] together provide strong support for the idea of a hydrothermally active Enceladus. The dominant source of H_2 in the plume is most likely hydrothermal processing of rock. The mineral and organic constituents of rock are likely intermixed such that H_2 production from mineral oxidation and organic pyrolysis may be coupled. The close association of minerals and organic matter, in conjunction with large-scale mixing inherent in hydrothermal circulation, offers the potential to understand the H_2/CH_4 ratio of the plume as a combination of sources [(*20*), section 4.3]. Hydrothermal circulation facilitates H_2 production by enabling more extensive water-rock interaction and provides

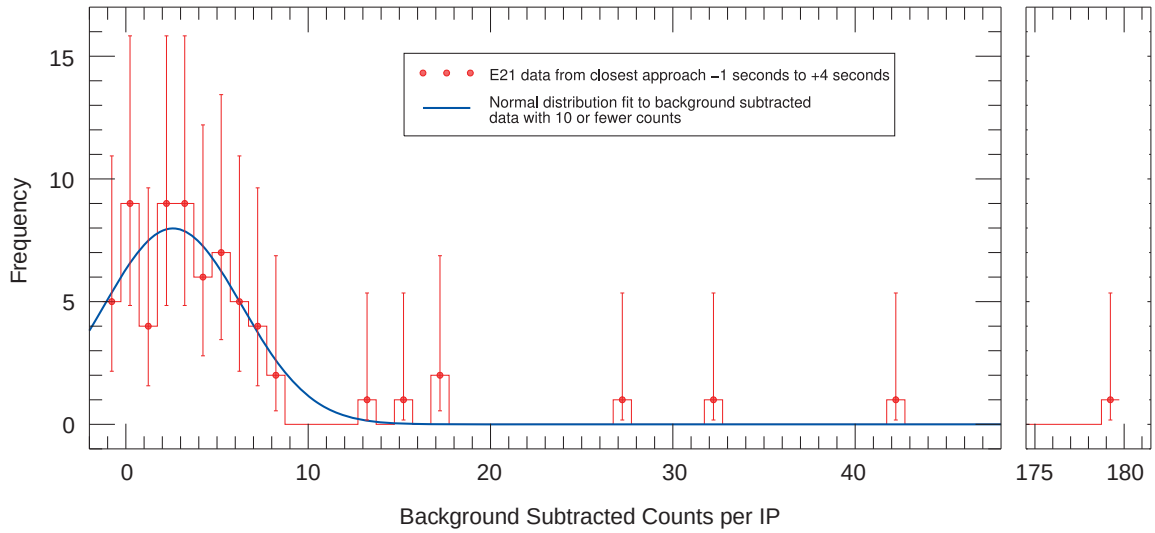

Fig. 3. Distribution of the background-subtracted data. This plot shows background-subtracted H_2 counts per IP (red) for a period of time from closest approach −1 s to +4 s that captures the portion of the H_2 measurements with the highest signal-to-noise ratio. The empirical distribution is compared to a normal distribution (mean, 2.6 counts; SD, 3.8 counts) fit to background-subtracted data with counts ≤ 10. Red bars depict Wilson score confidence intervals of 95%.

continual replenishment of H_2 to Enceladus' ocean. To explain the expression of hydrothermal geochemistry in the plume, we hypothesize that tidal dissipation occurs in Enceladus' core (*35*), creating permeable fracture pathways and thermal gradients that drive hydrothermal circulation (*36*).

Using H_2 to quantify disequilibrium between CO_2 and CH_4

Plume measurements of H_2 reported here, along with CO_2 and CH_4 reported earlier (*14*, *19*), are of broad interest because the methanogenesis reaction

$$CO_2(aq) + 4H_2(aq) \rightarrow CH_4(aq) + 2H_2O(l) \quad (1)$$

could provide a source of chemical energy to support the synthesis of disequilibrium organic materials (*4*). The feasibility of Eq. 1 in Enceladus' ocean can be determined from the chemical affinity of the reaction, which constitutes the amount of Gibbs energy that would be released if the reaction were to proceed (*3*). Energetically favorable (spontaneous or exergonic) reactions yield a change in Gibbs energy $\Delta G < 0$, corresponding to positive values for the chemical affinity.

The affinity can be calculated using textbook thermodynamic methodology [(*20*), section 5.2], but not without observational data for all of the species in Eq. 1. To enable estimates of the affinity in Enceladus' ocean, we developed a geochemical model that can be used to infer the concentrations of volatile species in the ocean from their plume abundances [(*20*), section 5.1]. The critical feature of this model is that it uses carbonate equilibria (*15*) to make a link between dissolved and gaseous abundances. From a modeling perspective, dissolved gas concentrations are dependent on pH and total dissolved carbonate (*25*) in the ocean as well as the ratios of H_2/CO_2 and CH_4/CO_2 in the plume. Because our calculations rely on model outputs rather than direct measurements of the ocean, we refer to derived affinities as apparent affinities.

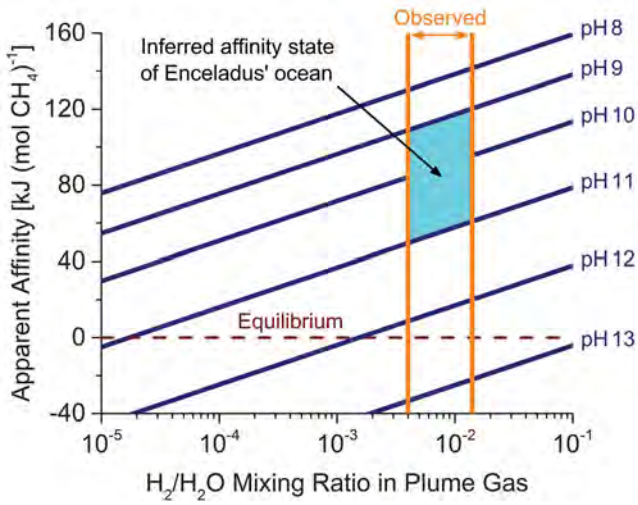

Fig. 4. Apparent chemical affinity for hydrogenotrophic methanogenesis in the ocean of Enceladus (273 K, 1 bar). The orange lines bracket the observed range in the mixing ratio of H_2 in the plume gas (Table 1). The dark blue lines are contours of constant ocean pH, a key model parameter. The cyan region indicates affinities for a pH range that may provide the greatest consistency between the results of (*13*, *15*, *25*). The dashed burgundy line designates chemical equilibrium, where no energy would be available from methanogenesis. These nominal model results are based on CH_4/CO_2 = 0.4 (Table 1), a chlorinity of 0.1 molal, and 0.03 molal total dissolved carbonate (*25*). Reported ranges in these parameters propagate to give an uncertainty in the computed affinities of ~10 kJ (mol CH_4)$^{-1}$.

Figure 4 maps out the affinity space for methanogenesis in terms of key environmental parameters at Enceladus. The apparent affinity is more positive at lower pH because of an increase in the concentration of dissolved H_2 in our model (table S11). For the observed range of H_2/H_2O ratios in the plume (~10^{-2}), it can be deduced that the affinity should be positive unless the ocean is highly alkaline (pH >12; Fig. 4). An upper limit for the pH, 13.5, has been reported (*15*), but such a high value seems inconsistent with Cassini CDA observations (*13*, *25*). A pH between ~9 and ~11 may provide the best reconciliation among previously reported values (*13*, *15*, *25*). In this pH range, we find large positive affinities [~50 to 120 kJ (mol CH_4)$^{-1}$].

It is apparent that the relatively high abundance of H_2 in the plume translates to a strong thermodynamic drive for methanogenesis in the ocean of Enceladus. This potential is independent of the source of H_2 because the Gibbs energy and chemical affinity are state functions. However, maintenance of a disequilibrium concentration of H_2 in an outgassing ocean implies a continual source (e.g., hydrothermal input). Our analysis supports the feasibility of methanogenesis as an energy-releasing process that can occur over a wide range of geochemical conditions plausible for Enceladus' ocean. This finding has implications for determining the habitability of Enceladus' subsurface ocean (*17*), although the favorable thermodynamics alone are

agnostic as to whether methanogenesis is actually occurring.

REFERENCES AND NOTES

1. N. H. Sleep, A. Meibom, T. Fridriksson, R. G. Coleman, D. K. Bird, *Proc. Natl. Acad. Sci. U.S.A.* **101**, 12818–12823 (2004).
2. T. M. McCollom, W. Bach, *Geochim. Cosmochim. Acta* **73**, 856–875 (2009).
3. E. Shock, P. Canovas, *Geofluids* **10**, 161 (2010).
4. J. P. Amend, T. M. McCollom, M. Hentscher, W. Bach, *Geochim. Cosmochim. Acta* **75**, 5736–5748 (2011).
5. K. Raymann, C. Brochier-Armanet, S. Gribaldo, *Proc. Natl. Acad. Sci. U.S.A.* **112**, 6670–6675 (2015).
6. J. B. Corliss *et al.*, *Science* **203**, 1073–1083 (1979).
7. D. S. Kelley *et al.*, *Nature* **412**, 145–149 (2001).
8. D. S. Kelley *et al.*, *Science* **307**, 1428–1434 (2005).
9. L. Iess *et al.*, *Science* **344**, 78–80 (2014).
10. W. B. McKinnon, *Geophys. Res. Lett.* **42**, 2137–2143 (2015).
11. P. C. Thomas *et al.*, *Icarus* **264**, 37–47 (2016).
12. O. Čadek *et al.*, *Geophys. Res. Lett.* **43**, 5653–5660 (2016).
13. H.-W. Hsu *et al.*, *Nature* **519**, 207–210 (2015).
14. J. H. Waite Jr. *et al.*, *Science* **311**, 1419–1422 (2006).
15. C. R. Glein, J. A. Baross, J. H. Waite Jr., *Geochim. Cosmochim. Acta* **162**, 202–219 (2015).
16. Y. Sekine *et al.*, *Nat. Commun.* **6**, 8604 (2015).
17. C. P. McKay, C. C. Porco, T. Altheide, W. L. Davis, T. A. Kral, *Astrobiology* **8**, 909–919 (2008).
18. J. H. Waite Jr. *et al.*, *Space Sci. Rev.* **114**, 113–231 (2004).
19. J. H. Waite Jr. *et al.*, *Nature* **460**, 487–490 (2009).
20. See supplementary materials.
21. B. D. Teolis *et al.*, *Space Sci. Rev.* **190**, 47–84 (2015).
22. J. I. Lunine, D. J. Stevenson, *Astrophys. J. Suppl. Ser.* **58**, 493 (1985).
23. W. L. Mao, H. K. Mao, *Proc. Natl. Acad. Sci. U.S.A.* **101**, 708–710 (2004).
24. C. J. Hansen *et al.*, *Geophys. Res. Lett.* **38**, L11202 (2011).
25. F. Postberg *et al.*, *Nature* **459**, 1098–1101 (2009).
26. F. Postberg, J. Schmidt, J. Hillier, S. Kempf, R. Srama, *Nature* **474**, 620–622 (2011).
27. C. R. Glein, E. L. Shock, *Geophys. Res. Lett.* **37**, L09204 (2010).
28. H. Balsiger *et al.*, *Sci. Adv.* **1**, e1500377 (2015).
29. A. Bar-Nun, D. Prialnik, *Astrophys. J.* **324**, L31–L34 (1988).
30. J. Telling *et al.*, *Nat. Geosci.* **8**, 851–855 (2015).
31. B. Sherwood Lollar, T. C. Onstott, G. Lacrampe-Couloume, C. J. Ballentine, *Nature* **516**, 379–382 (2014).
32. C. C. Blair, S. D'Hondt, A. J. Spivack, R. H. Kingsley, *Astrobiology* **7**, 951–970 (2007).
33. B. Sherwood Lollar, T. D. Westgate, J. A. Ward, G. F. Slater, G. Lacrampe-Couloume, *Nature* **416**, 522–524 (2002).
34. G. Proskurowski, M. D. Lilley, D. S. Kelley, E. J. Olson, *Chem. Geol.* **229**, 331–343 (2006).
35. J. H. Roberts, *Icarus* **258**, 54–66 (2015).
36. B. J. Travis, G. Schubert, *Icarus* **250**, 32–42 (2015).

ACKNOWLEDGMENTS

Supported by the Cassini INMS subcontract from NASA JPL (NASA contract NAS703001TONM0711123, JPL subcontract 1405853); INMS science support grant NNX13AG63G (M.E.P.), and JPL subcontract 1437803 (J.I.L.). J.H.W. thanks L. Jones of Boeing for a helpful statistical discussion, and S. Kempf and F. Postberg for sharing the Cassini Cosmic Dust Analyzer results from E21 that were taken into consideration in the data analysis. C.R.G. thanks the Deep Carbon Observatory community for numerous informative discussions on planetary applications of deep energy. The spacecraft data used in this paper are available from the NASA Planetary Data System archive at http://ppi.pds.nasa.gov/search/view/?f=yes&id=pds://PPI/CO-S-INMS-3-L1A-U-V1.0/DATA/SATURN/2015/274_304_OCT/301. Our simulation, modeling, and calibration codes and data products are available at https://inms-support.space.swri.edu/.

SUPPLEMENTARY MATERIALS

www.sciencemag.org/content/356/6334/155/suppl/DC1
Materials and Methods
Supplementary Text
Figs. S1 to S12
Tables S1 to S11
References (*37–103*)

23 August 2016; accepted 20 March 2017
10.1126/science.aai8703